

The design of a test rig and study of the performance and efficiency of a Tesla disc turbine

G P Hoya and A Guha*

Aerospace Engineering Department, University of Bristol, University Walk, Bristol, UK

The manuscript was received on 25 June 2008 and was accepted after revision for publication on 18 December 2008.

DOI: 10.1243/09576509JPE664

Abstract: A Tesla disc turbine and a flexible test rig have been designed and manufactured, and experimental results are presented. An analysis of the performance and efficiency of the disc turbine is carried out. The design philosophy of the flexible test rig has been explained. Various complementary methods of measurement have been implemented and compared, and several operational experiences have been noted. A new simple method, the angular acceleration method, for measuring output torque and power in a Tesla turbine has been developed. This proved to be a successful method for overcoming the difficulties associated with the determination of very low torque at very high angular speed.

Keywords: disc, turbine, bladeless, Tesla, shear force, eddy-current brake, torque, power, efficiency

1 INTRODUCTION

In this article, we describe the design and manufacture of a disc turbine and of a flexible test rig for a systematic study of its performance, and report some sample results. A disc turbine is a type of bladeless turbomachinery that works by means of shear forces produced by the action of the fluid passing through the narrow gaps between a set of coaxial discs. It is also called a Tesla turbine, named after its inventor Nikola Tesla (1856–1943), who is well known for his research and inventions related to electricity and induction motors. However, in 1913 he patented a revolutionary motor, consisting of a bladeless turbine [1]. This turbine was formed of a series of flat, parallel, co-rotating discs, closely spaced and attached to a shaft, forming a rotor. The rotor rotated within a housing, with a small radial and axial clearance. The working fluid was injected in a direction nearly tangential to the rotor by means of an inlet nozzle, and exhausted through outlet ports in the discs near the shaft. Tesla's engine had the advantage that it could also be used as a compressor, by powering the rotor with an external motor and modifying the housing [2]. The direction of flow was thus inverted,

flowing outwards and exhausting tangentially into a spiral volute. The reported power output of the first turbine developed by Tesla was 30 hp; this machine had eight discs of 6 in diameter, and was powered by compressed air [3]. Some years later, he built a new turbine with an 18 in diameter rotor, which reached 200 hp using steam as the working fluid [3].

However, the lack of interest from contemporaries and the impossibility for Tesla to finance himself put a stop to his development of the bladeless turbine. Nevertheless, this engine was not forgotten and studies have been carried out about its working from the 1950s [4] onwards.

In 1952 Armstrong [5] built a ten-disc Tesla turbine that reached 1.11 hp and an efficiency of 14 per cent. Later, in 1965, Rice [6] conducted research on multiple-disc turbines and developed several turbomachines. Other authors, such as Beans [7], also investigated the bladeless turbine. However, the maximum power reached by any of these new turbines was much lower than those obtained by Tesla, generally being below 2 hp, and the efficiency fluctuated between 20 and 35 per cent.

According to Cairns [3], the working principle of Tesla turbomachinery can be explained by analogy to the movement of a fluid within a pipe. When a fluid flows within a pipe, the friction with the wall of the pipe due to the viscosity of the fluid results in the wall being dragged along by the fluid; consider what would

*Corresponding author: Aerospace Engineering Department, University of Bristol, University Walk, Bristol, BS8 1TR, UK.
email: A.Guha@bristol.ac.uk, guha.a@rediffmail.com

happen if the pipe's movement was not constrained. If instead of a pipe, the fluid flows within two flat parallel plates, it would make them accelerate until they reach the velocity of the fluid. Therefore, if these plates have the shape of a disc, and these discs are mounted on a shaft, forming a rotor, the fluid passing between the gaps would make the rotor spin, accelerating to reach the speed of the flow. At the same time that the rotor accelerates, fluid velocity decreases from the maximum at the periphery while it flows spirally inwards up to the central exhaust ports. This effect is due to the fact that the kinetic energy of the fluid is transformed into the work available at the shaft [3]. As explained by Hasinger and Kehrt [8], the relative velocity between the driving medium and the driven medium should be small, in order to achieve an efficient Tesla turbomachine. Most authors agree that the Tesla turbine is an *almost pure impulse turbine*, i.e. there is a large pressure drop in the nozzle and a small pressure drop in the rotor.

To sum up, the Tesla turbine produces an exchange of momentum by the use of the friction of the fluid passing through the gaps between the discs [7]. As the angular velocity of the rotor increases, the viscous shear force decreases, thereby decreasing the output torque. The rotor reaches a steady angular speed when the output torque is balanced by the sum of externally applied load and various losses in the system (e.g. friction at the bearings, leakage flow through the clearance gap between the rotor and housing, etc.).

The most important parameters that affect the performance and efficiency of disc turbomachinery, as outlined by Cairns [3] and Rice [4], are as follows:

- (a) spacing between the discs;
- (b) characteristics of the fluid and the flow, such as velocity ratio;
- (c) conditions of the surfaces of the disc and radius ratio;
- (d) radial and axial clearances between the rotor and the housing.

After the success of Whittle and von Ohain, the gas turbine became the centrepiece of research and development and the understanding of its performance and optimization has reached quite a mature stage [9–15]. The understanding of the performance of Tesla turbines is not nearly as thorough. Recently, several references have been written [3, 16–20] on Tesla turbines; however, they usually describe the studies we have mentioned above and do not include any new experimental results.

An important advantage of the Tesla turbine is that its construction is simple and it can be manufactured in a local workshop. We therefore decided to build a Tesla turbine, develop a flexible test rig and undertake a systematic study of the performance of the turbine (particularly in the context of non-availability

of modern experimental studies). The objectives of the current study are as follows.

1. To design and manufacture a disc turbine.
2. To design, manufacture and develop a flexible test rig for the Tesla turbine, which, if possible, can also be used for testing Tesla compressors. This would entail the consideration and evaluation of various measuring techniques overcoming the principal difficulties that are associated with measurements in a small Tesla turbine, viz. the determination of very low torque at very high angular speed. If feasible, more than one method would be used to measure a quantity so that consistency can be checked.
3. To conduct a systematic study of the performance of Tesla turbines.

2 CHARACTERISTICS OF THE TURBINE AND ITS HOUSING

A multiple-disc turbine has been initially designed as the first representative turbine for detailed experimental investigations, and it is planned to design and build a few more turbines in the future to study aspects such as the effects of scaling. The overall features of this first turbine were chosen according to the experience noted in the references [1, 3, 4, 7, 16, 21]. The disc diameter is 92 mm (3.6 in), the thickness of each disc is 0.9 mm, and the rotor-to-housing diametrical clearance is 0.3 mm. An overall view of the turbine can be seen in Fig. 1(a). The discs have a single central outlet port, since this configuration was found to be more efficient by Davydov and Sherstyuk [21] and Rice [4]. The diameter of this central hole is 25 mm. In order to accommodate the outlet of the fluid, the shaft is supported as a cantilever by means of bearings inside the base plate (Fig. 1(a)). The rotor is formed from the selected number of individual discs by keeping them together with the help of three locating pins built-in on to a thicker master disc attached to the shaft. Immediately after the master disc, two discs are put together with no spacing between them. The purpose is to use them as the thicker end discs as used by Tesla [1]. They do not contribute to the momentum transfer between the fluid and discs but prevent the air, injected by the nozzle, from moving out of the rotor instead of entering in the gap between the discs [1, 16, 17]. The whole stack of discs is fixed to the master disc by using three bolts, as can be seen in Fig. 1(b). Hence, a total of six pins go through the rotor, which is shrouded by the housing. Then, the housing is bolted and sealed to the base plate.

The shaft of the turbine is extended beyond the base plate; this makes it possible to attach two discs to the shaft outside the housing. The first one is a small disc, which, together with an optical sensor, is

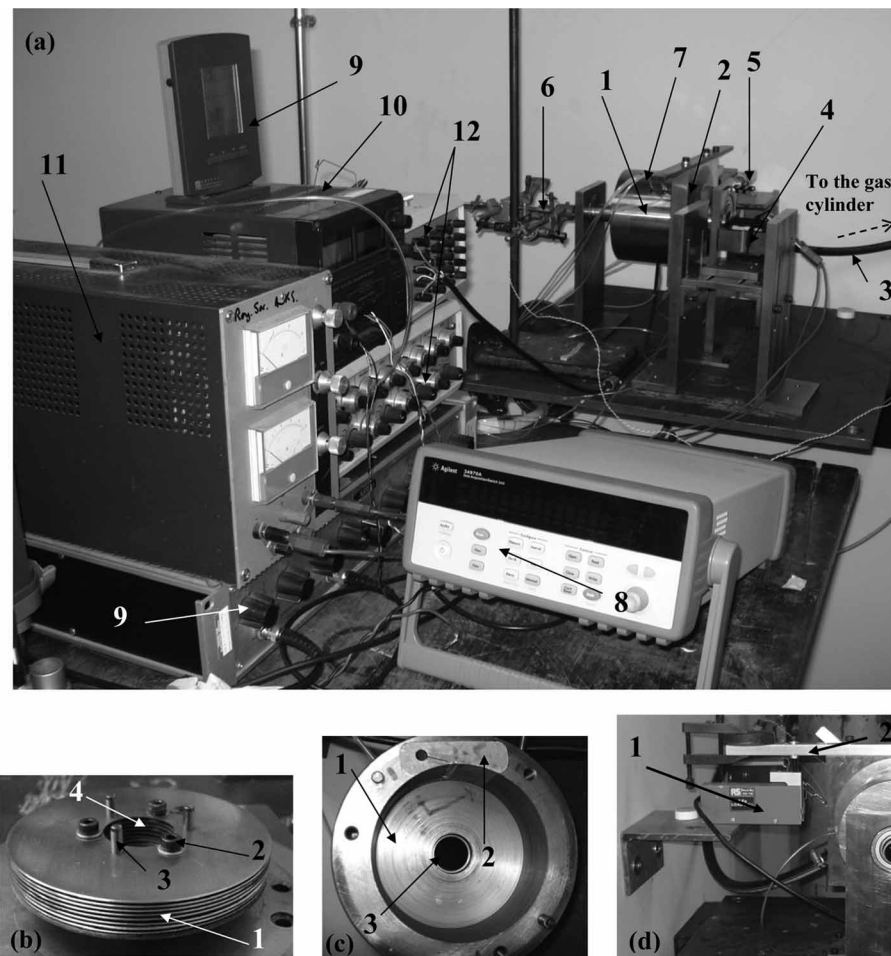


Fig. 1 (a) Overall view of the test rig and the turbine. Keys: (1) turbine housing, (2) base plate, (3) inlet pipe, (4) eddy-current brake, (5) optical sensor, (6) outlet Pitot tube, (7) pressure tapplings of the housing, (8) data logger, (9) barometer, (10) power supply for the optical sensor, (11) power supply for the electromagnet, and (12) strain gage amplifier. (b) Details of the turbine's rotor. Keys: (1) discs, (2) bolt, (3) locating pin, and (4) exhaust port. (c) Details of the turbine's housing. Keys: (1) end wall of the housing, (2) nozzle insert, and (3) outlet. (d) Mechanism to measure the reaction torque. Keys: (1) load cell and (2) reaction arm

used to measure the angular velocity of the rotor. The other disc is larger and forms part of an eddy-current brake. Moreover, the extended shaft allows the use of other methods for the measurement of output power as well as the attachment of a driving device to power the rotor, so that just by designing and manufacturing a new housing the turbomachine could be used as a compressor, maintaining the same rotor and the base unit. This enhances the flexibility of the test rig.

The turbine itself is also very flexible in the current design since various parameters can be easily varied in order to study their effects on the performance and efficiency of the turbine. It is possible to change the number of discs, disc spacing, and geometry of the nozzle without changing the base plate, end plate, or the housing. The disc spacing is varied by means of a number of 0.2 mm thick washers placed on the three

locating pins (see the first paragraph of section 2). The geometry of the nozzle can be changed, thanks to the use of an interchangeable nozzle insert. This nozzle insert can be seen in its position in the housing in Fig. 1(c) and its geometry is outlined with more details in Fig. 2(a). The width of the slot-shaped nozzle can be adapted to the different widths of the rotor by using inserts with the shape of the nozzle channel, so that the unused area of the nozzle can be blocked and the jet can be directed more efficiently to the rotor and major leakages can be avoided.

The fluid passes from the central hole of the discs into an exhaust pipe that runs through the end wall of the housing. The pipe can be moved axially inwards or outwards so that its end can be adjusted with respect to the central hole of the discs. This variable position of the exhaust pipe was included in the design

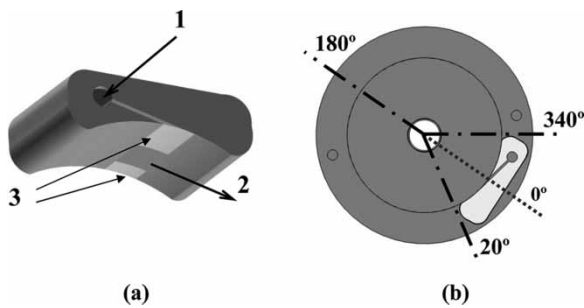


Fig. 2 Scheme of the air injection system of the Tesla turbine. (a) CAD model of a nozzle insert. Keys: (1) direction of entrance of the flow, (2) direction of injection of the jet in the rotor, and (3) blockings of the end of the nozzle slot. (b) Positions of sets of pressure tapplings with regard to the outlet of the nozzle (0°)

since the end wall of the housing remains in a fixed position, but the axial extent of the rotor assembly changes according to the number of discs used (which is variable).

3 TEST RIG AND MEASUREMENT TECHNIQUES

A test rig was developed to measure the various parameters that are necessary to determine the performance and efficiency of the Tesla turbine. Most of the apparatus used is outlined in Fig. 1(a). Gas cylinders containing compressed air are used to provide high-pressure air at the inlet of the nozzle. A pressure regulator, situated immediately after the gas cylinder, controls the inlet total pressure, which is usually in the range of 2–4.5 bar. Static and total pressures at various locations are read and logged by a ZOC 22B Scanivalve [22]. Temperatures, rotation per minute, and force measured in an RS 632–736 Load Cell are logged by an Agilent 34970A Data Logger [23].

The fluid flows through a flexible pipe from the pressure regulator into the housing. Total pressure, static pressure, and total temperature are measured at the inlet duct before the turbine. To do this, a type-K thermocouple is placed at the beginning of the inlet pipe, and a Pitot tube and a pressure tapping are placed in a fitting right before the entrance to the inlet nozzle. Total pressure and total temperature are measured again at the outlet of the turbine.

Inside the housing, several pressure tapplings are set in order to know the static pressure distribution in the chamber. Altogether nine tapplings are used at three circumferential positions (see Fig. 2(b)), each set at three axial planes. The first two planes are covered by the jet of the nozzle, whereas the third set is placed close to the end wall inside the housing. The purpose of the two sets covered by the width of the jet is to

estimate the static pressure at the outlet of the nozzle, since it was not possible to directly measure the pressure exactly at that position.

The flexibility of the turbine designed for this research with regard to the number of discs and disc spacing entails a problem: the sealing between the end plates of the housing and the rotor is not assured. This problem was faced by blocking the ends of the nozzle slot, as explained before. However, it was decided to check whether this was actually working; to do this, a set of three tapplings was placed at the end of the housing. This allowed one to know the pressure distribution there, as well as to compare the pressures with those obtained in the area covered by the jet of the nozzle by means of the other two sets of tapplings. The results are discussed in section 6.

3.1 Determination of output power

3.1.1 Direct measurement of output power

In the test rig used in this research, the power output can be obtained directly by means of an electric generator connected to the shaft of the turbine. A suitable motor that is sold in the market as a standard carpentry tool was identified and some changes in the electrical connections were made in-house so that it could act as a generator. This generator could reach maximum speeds up to 30 000 r/min and thus was initially considered suitable for the present purpose (the high revolutions per minute of the Tesla turbine may restrict the use of other power and torque measurement devices). The kinetic energy of the shaft is converted into electric energy, which can be measured by determining the voltage and current. Hence, the power can be calculated as $P = v \cdot i$.

The use of the electrical generator has an additional advantage in the flexibility that it offers, because the electrical machine can be run as a motor to drive a Tesla compressor (with some suitable modifications of the housing). However, the measured power would include any frictional losses in the bearings of the turbine shaft and the electrical generator itself. It was found that the frictional torque in the electrical generator was high compared with the torque produced by the present Tesla turbine; hence this method was, in the end, not used for determining the final results of the current study.

3.1.2 Determination of power from torque and angular speed

Apart from the direct measurement of power, it can also be calculated from equation (1) once the torque and angular velocity are known

$$P = \tau \omega \quad (1)$$

In the following, a method for determining angular speed and several methods for determining the output torques that have been used in the present investigation are described.

3.2 Determination of angular speed by an optical sensor

The angular speed ω was obtained by means of an optical sensor, which can be seen in Fig. 3. The methodology for the use of this device is simple. A disc with two through holes is attached to the shaft, so that as this wheel rotates within the gap of the sensor a frequency output is obtained, which is then converted to angular velocity in the data logger. As there are two holes, the software of the data logger was programmed to divide the frequency readings by two, in order to obtain the actual angular speed. A handheld tachometer was used once to double-check the readings obtained by the optical sensor and the two measurements were consistent.

The optical sensor required a power supply, which can be seen in Fig. 1(a). This method was found to be accurate and inexpensive. The angular velocity obtained was used in two different ways: First, ω is needed to determine the power from equation (1), i.e. $P = \tau\omega$. Second, the time evolution of ω is also used in the acceleration method, described in section 3.3, to determine the torque τ as well.

3.3 Torque and power output measurement under unsteady state: angular acceleration method

According to Newton's second law of motion, the torque produced by the disc turbine can be calculated as the product of moment of inertia of the rotating

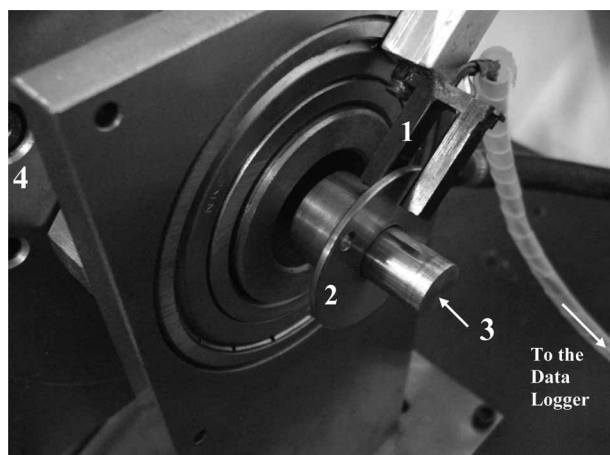


Fig. 3 Apparatus used to measure the angular velocity of the rotor. Keys: (1) optical sensor, (2) disc with two through holes, (3) turbine shaft, and (4) base plate

parts and the angular acceleration

$$\tau = I\alpha \quad (2)$$

The angular acceleration is obtained by numerically differentiating the angular velocity of the disc attached to the shaft, measured by the optical sensor. The speed is measured during the acceleration phase (when compressed air is being injected into the turbine) as well as during the deceleration phase, when the supply of compressed air is switched off after the rotor reaches its maximum speed and the turbine rotates by the effect of the inertia. According to Newton's first law of motion, the rotor should maintain a constant speed under this situation unless there is a resistive, dissipative force (in the form of friction). The resistive force gives rise to a frictional torque, which tends to decelerate the rotor. It is assumed here that, at the same rotational speed, the frictional torque operative under the acceleration phase (when the supply of compressed air is on) is the same as that operative under the deceleration phase (when there is no supply of compressed air and the friction is acting on its own). Therefore, if one measures the frictional torque during the deceleration phase and the net accelerating torque during the acceleration phase, then one can write that, at any particular rotational speed, *actual torque* produced by the turbine = net accelerating torque + frictional torque. Then, according to equation (1), the power can be calculated as $P = \tau_{\text{actual}}\omega = (\tau_{\text{accelerating}} + |\tau_{\text{frictional}}|)\omega$.

From equation (2) it can be deduced that it is crucial to calculate the moment of inertia as accurately as possible for an accurate determination of the torque. Since the geometry of the shaft and the rotor assembly is very complex, the moment of inertia was calculated by means of the CAD files used for manufacturing the turbine, and the results were checked later by hand calculations on a simplified geometry. The numerical differentiation of angular velocity versus time to obtain angular acceleration can be tricky if the actual experimental values at discrete levels of time do not form a smoothly varying function. In this work, the angular velocity was therefore first expressed as a function of time by a high-order polynomial curve-fit through the data points. This algebraic polynomial expression was then differentiated analytically to generate the variation of angular acceleration with time. Moreover, the angular acceleration was also determined by direct numerical differentiation in finite-difference form. The two results agreed closely, indicating that the velocity measured by the optical sensor was smoothly varying and of good quality.

3.4 Tests under steady state: eddy-current braking

In order to make it possible to reach a steady state (i.e. to maintain a constant angular speed while

varying other parameters), an eddy-current brake was designed, manufactured, and implemented to load the shaft of the turbine. When considering the different possibilities to achieve the steady state, three methods were initially found: friction braking, regenerative braking, and magnetic braking.

When testing machines such as internal combustion engines, the most usual method to load the shaft is to use a brake pad, in other words, *friction braking*. In this way, by changing the braking force applied to the brake, the angular speed is reduced until a constant speed is reached. However, this method is not suitable for the current disc turbine, since the angular speeds reached are extremely high and the braking pads would wear out quite quickly. Moreover, the braking performance of this kind of brake is low in a high-speed region [24]. Therefore, this method was ruled out. The next method considered was the use of *regenerative braking*. This method consists of connecting an electric generator to the shaft, so that by measuring the current and voltage created, the power output can be determined (see section 3.1(a)). However, the torque generated by the disc turbine was not high enough to overcome the resistance torque of the electrical generator, so this method had to be ruled out too.

The best method for the present purpose was found to be the use of a *magnetic brake* or *eddy-current brake*. This kind of brake consists of a non-ferromagnetic disc attached to the shaft and a magnet or electromagnet between whose poles the disc rotates. It permits the loading of the shaft without any wearing, since there is no contact between the disc and the poles, and the braking torque is controllable by varying the input current of the electromagnet, so it can be adapted to the low torque produced by the disc turbine. Figure 4 shows the eddy-current brake set used in the test rig, which consists of an electromagnet, a disc, and a base for the electromagnet. This base was designed and manufactured so that it can act as a flexible holding platform for the electromagnet, which would work with various sizes of the Tesla turbine or various sizes of the electromagnet itself. The critical functional requirement is that the disc of the eddy-current brake is fixed to the shaft of the Tesla turbine; the flexible design of the base allows changing the vertical and horizontal position of the electromagnet, in order to easily adjust it and adapt it to possible future changes in the test rig.

The design of the disc was a crucial part of the design of the brake, since the disc had to overcome the centrifugal forces acting on it as a result of the high angular velocity, i.e. it must be safe to use it, but also had to provide the appropriate braking torque. As far as the former requirement is concerned, according to Faupe [25], the allowable speed of a rotating hollow disc

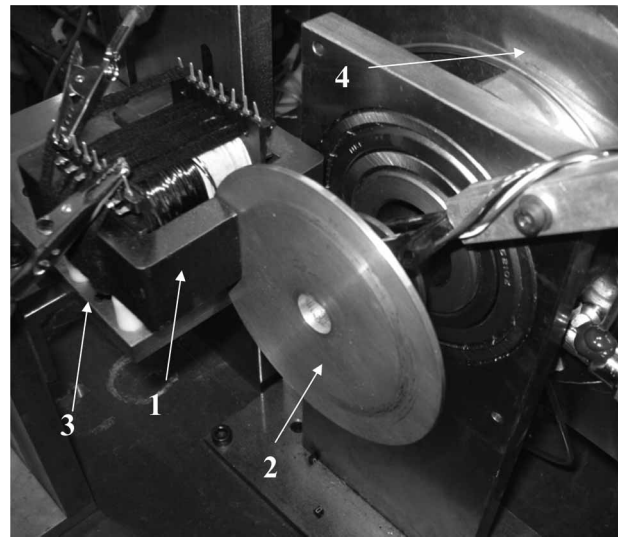


Fig. 4 Eddy-current brake. Keys: (1) electromagnet, (2) disc, (3) base for the electromagnet, and (4) base plate of the turbine

of constant thickness is

$$\omega_{\text{allowable}} = \sqrt{\frac{8g\sigma_w}{(3+\nu)\rho r_o} \left(\frac{1}{2 + (r_i/r_o)^2 [1 - (1+3\nu)/(3+\nu)]} \right)} \quad (3)$$

The angular speed given by equation (3) is the maximum at which the disc can be rotated without the risk of plastic deformation or bursting. In equation (3), σ_w is the working stress, defined as $\sigma_w = \sigma_y/Sf$. For the current design, the material selected was an aluminium alloy used in aerospace applications and a safety factor (Sf) of 1.5 was used.

According to Lee and Park's theory [24], the braking torque produced by the eddy-current brake is given by

$$\tau_b = \tau_i i^2 \omega \quad (4)$$

where

$$\tau_i = \beta C \sigma \mathfrak{N}^2 S d \left(\frac{\mu_0 \cdot N}{l_g} \right)^2 \quad (5)$$

$$\beta = 1 - \frac{1}{2\pi} \left[4 \tan \left(\frac{b}{a} \right) + \frac{b}{a} \ln \left(1 + \frac{a^2}{b^2} \right) - \frac{a}{b} \ln \left(1 + \frac{b^2}{a^2} \right) \right] \quad (6)$$

$$C = \frac{1}{2} \left[1 - \frac{ab}{\pi(1 + \mathfrak{N}/r)^2 (r - \mathfrak{N})^2} \right] \quad (7)$$

The braking torque was calculated by means of equation (4) for several outer radii of the discs. By comparing this torque with that obtained experimentally

by the turbine for several angular velocities (by the angular acceleration method described in section 3.3), a compromise was reached for the outer radius of the disc taking into account the allowable speed calculated using equation (3).

This is one of the most used relations that can be found in the literature, but it has a limitation in that the calculated braking torque matches accurately with the actual braking torque only at low angular speeds, since the relationship between braking torque and angular speed is, in reality, non-linear at high speeds [26], whereas Lee and Park's theory (equation (4)) gives a linear relationship. The reason for the different behaviour of the eddy-current brake in the low- and high-speed regions is that, according to Simeu and Georges [27], at high speed the magnetic induction created by the electromagnet is partially cancelled by that created by the eddy currents, which makes the net magnetic induction decrease and hence the braking torque also decreases. According to Anwar [26], at high speed the relationship between braking torque and angular speed can be expressed as a second-order polynomial $\tau_b = f_0 + f_1 i + f_2 i^2$, where each of f_0 , f_1 , and f_2 are various second-order polynomials in ω . Although this method gives a more accurate prediction for the braking torque, nine constant coefficients are needed to specify f_0 , f_1 , and f_2 , and can only be determined by conducting experiments on an existing disc if another independent method of torque measurement is available (the coefficients need to be determined only once; thereafter the equation has predictive power). Therefore, for the preliminary design of a brake, one is forced to use a more self-contained theory and, hence, Lee and Park's theory was used here for the preliminary design even at high-speed conditions.

Another important parameter when designing the eddy-current brake was to find out the number of turns N for the coil of the electromagnet. A suitable value of N , for a desirable range in current i , may be estimated from equation (5) for a braking torque higher than that actually desired (since it was going to be lower actually, due to the inaccuracy of Lee and Park's theory for a high-speed region). Moreover, if it was later found that the calculated number of turns was too low, more turns could be added to the electromagnet.

3.5 Shaft power measurement: reaction torque method

An interesting characteristic of the design of the disc turbine used in this research is that the whole machine is supported on bearings along the same axis as the shaft, so that it is free to rotate. This freedom can be resisted by attaching a reaction arm to the housing, its movement being stopped by a load cell. The reaction-arm-load-cell mechanism can be seen in Fig. 1(d). It uses Newton's third law of motion; the torque of the

turbine produces an equal and opposite torque in the housing, necessary to hold the drive and the driven equipment in place [28]. This reaction torque can be obtained by multiplying the force measured by the load cell and the length of the moment arm. The electric signal from the load cell is conducted to a strain gage amplifier, then to a low-pass filter, and finally it is logged in the data logger. However, some problems were found in the application of this method, as explained in section 4.3.

4 OPERATIONAL EXPERIENCE

4.1 Inlet

During the research dealt with in this article, it was found that it is very important to analyse the validity of the pressure readings at the inlet of the turbine [29]. Care is needed in designing the measurement positions for the total pressure and temperature at the inlet. It was found that our flexibility in changing the nozzle quickly by the use of interchangeable inserts caused some restriction in the flow-path design at the inlet. This operational experience has given us the guidance for an improved design in future. Second, it was found (see section 6) that a good design of the nozzle is important in improving the overall efficiency of the turbine. The mass flow at the inlet is estimated by the laws of gas dynamics (section 5) by measuring the total pressure, total temperature, and static pressure at a location in the inlet pipe. Given the importance of the mass flowrate in determining the performance parameters of the disc turbine, an independent measurement of the mass flowrate would be desirable in the future development of the project.

4.2 Outlet

After the nozzle, the fluid flows spirally inwards through the disc spacings; shear forces cause an exchange of momentum between the fluid and the discs and make the rotor rotate. The fluid bends by 90° at the central holes of the discs and exhausts to the atmosphere through a pipe connecting the interior of the housing with the exterior, as explained in section 2.

Initially in this investigation, the conditions at the exhaust were measured by means of a Pitot-static tube and a type-K thermocouple attached to it. This allowed the determination of total pressure, static pressure, and total temperature at the outlet of the disc turbine. However, problems were found in both the pressure and temperature measurements. As far as the total temperature at the exhaust is concerned, a critical problem was found in its measurement: the temperature at the outlet was higher than that at the inlet. Obviously this is not realistic, since the total temperature should not increase after a process in which work

is extracted from the fluid (the thermocouples having been correctly calibrated).

In the test rig, the thermocouple that measured the outlet total temperature was stuck to the Pitot-static tube, and the depth at which this probe could be introduced in the exhaust pipe was limited by an elbow. Therefore, the parameters were not being measured right after the discs, but quite far away from them. Due to the complexity of the flow at the exhaust and the significant temperature difference with the environment, a temperature recovery could be occurring. Hence, it was decided to place the thermocouple closer to the actual exhaust of the rotor. In order to do this, the Pitot-static tube that was used initially was discarded and a new Pitot-static tube was employed. The advantage of this new probe is that it is straight, i.e. it does not have bends or elbows, so that it could be introduced completely through the exhaust pipe up to the actual exhaust of the rotor. The thermocouple was then stuck to this new Pitot-static tube. With this new layout, the results changed significantly. Now the outlet total temperature was lower than that at the inlet (however, the output power calculated from the difference of the inlet and outlet total temperatures is still significantly different from the output power measured by the acceleration method (section 3.3)).

With regard to the pressure measurements, it was found in reference [28] that the measured total pressures seem to vary significantly at different points of the cross-section of the outlet pipe, and the measured total pressure appeared to be lower than the static pressure, which is not realistic. These difficulties had not been described in the literature consulted. It was thought that this problem would be solved by means of a longer Pitot-static tube described above, which allowed the measurement of pressures directly after the rotor. However, this did not solve the problem. *The flow at the exhaust is very complex* and seems to follow a spiral path through the exhaust pipe. It is thought that a possible cause for this behaviour of the pressure readings could be the fact that the probe is misaligned relative to the direction of the flow. Then, the air is directed more directly to the static taps rather than to the total pressure tap of the Pitot-static tube.

In reference [30] it is seen that Pitot tubes with a conical nose are more sensitive to misalignment than those with a cylindrical external shape. Moreover, the sensitivity to misalignment of the latter can be reduced further if they have a 15° internal chamfer [30]. A Pitot tube with these characteristics was manufactured and the thermocouple was stuck outside the tube. The measured pressures with this modified Pitot tube were higher than the static pressures measured in other tests, and for the first time were also higher than the atmospheric pressure. Unfortunately, it cannot be said that this happened always; hence the effectiveness of this new Pitot is not completely demonstrated.

Moreover, although the measurement of the total pressure at the outlet was improved, this probe did not have static taps.

To sum up, it has been found that both temperature and pressure readings at the outlet of the particular turbine under consideration are difficult to obtain accurately and the flow may not be suitable for a quasi-one-dimensional gas dynamics analysis. Further research is needed to find out the nature of this exhaust flow; accurate values of the total pressure at exhaust are critical in defining the isentropic efficiency of the Tesla turbine.

4.3 Reaction torque method

This method has been proposed by Drecq [31], Gindy [32], and Fleming [33], but none of the references give detailed descriptions for practical implementation of the method. This method has been implemented in the present study (see section 3.4), but two problems were found. First, the flexible pipe (responsible for providing compressed air to the turbine) connected to the base plate applied a certain amount of reaction torque, which is not negligible as compared to the low value of torque provided by the turbine (this was verified by measuring the force on the load cell with and without the flexible pipe in position). Second, the transmission of the force between the reaction arm and load cell was more complex than expected; it was found that the readings depended strongly on the nature of connection between the reaction arm and the load cell. Several attempts were made in order to obtain accurate readings from the load cell (which was calibrated properly) by changing the way of connecting it to the arm. First, a pin was placed at the lower side of the tip of the reacting arm, the pin resting freely on the load cell plate. So when the turbine produced power and the reaction arm wanted to move downwards, the reaction force got transmitted to the load cell. However, the pin and the reaction arm could go up and detach from the load cell plate when a vibration was present. Moreover, the readings were not repeatable, i.e. if a load was applied on the arm and after that the load was removed, the measurement of the load cell was not the same; it did not return to zero. At first it was thought that the problem may be a result of the friction between the tip of the pin (connected to the arm) and the plate of the load cell. An attempt was made to reduce this friction by attaching a wheel at the bottom of the pin, but this did not remove the problem with repeatability.

When the reaction arm was attached to the plate of the load cell by screwing the pin into a threaded hole on the plate, it was found that this restricted completely the movement of the mechanism, and no force could be measured. A last attempt was made to solve the problems with vibration and repeatability.

This involved the design and manufacture of a linkage between the reaction arm and the load cell. A pin was screwed to the reaction arm and another pin was screwed into the plate of the load cell, and a third link was placed in the middle connected through pin joints at both ends to the pins connected to the reaction arm and load cell, respectively. Therefore, this mechanism allowed a horizontal movement of the reaction arm with regard to the load cell, whereas the vertical movement was transmitted to and measured by the load cell. However, this linkage also did not solve the difficulties mentioned before, and inaccuracies still exist in the reaction torque measurement.

4.4 Disc rubbing

According to Cairns [3], Tesla's turbines were not persisted upon by the Allis Chalmers Company (the first company that was interested in this turbomachine and manufactured some of the most powerful Tesla turbines) because of the finding that the discs had stretched as a result of inertial forces. This problem has not been described again by any of the authors in the cited literature. However, in the current research it was found that some discs had sometimes rubbed with the housing. The problem seemed to occur only for speeds $>10\,000$ r/min and when more than four discs were being used. We performed some preliminary calculations for the allowable angular speed from stress considerations with the help of equation (3) and for the disc stretching using the related theoretical formulation. Such simple calculations show that disc stretching should not cause any rubbing in the present case. The test rig, however, showed noticeable vibration at very high angular speeds and when a large number of discs were used. It is thought that this was possibly responsible for the rubbing marks. Only four discs were used for producing the results given in this article, for which vibration (or disc rubbing) was not a problem.

5 CALCULATION PROCEDURES

A steady, adiabatic, compressible, quasi-one-dimensional flow of a perfect gas is assumed.

5.1 Inlet: mass flow and power input

The mass flow was estimated by means of the total and static pressures and total temperature readings at the inlet duct before the turbine. The Pitot tube at that position brings the fluid to rest, making it possible to obtain the total pressure. This process is considered adiabatic and reversible [34], i.e. isentropic. Then, knowing the static-to-stagnation pressure ratio and the stagnation temperature, the velocity of the fluid can be calculated. From the steady flow energy

equation it is obtained as

$$T_0 = T \left(1 + \frac{\gamma - 1}{2} M^2 \right) \quad (8)$$

Since the process is assumed to be isentropic, the Mach number and the velocity of the fluid at the point where pressures and temperatures are being measured are respectively

$$M = \sqrt{\frac{2}{\gamma - 1} \left[\left(\frac{p_0}{p} \right)^{(\gamma-1)/\gamma} - 1 \right]} = f(p_0, p) \quad (9)$$

and

$$V = \sqrt{2c_p T_0 \left[1 - \left(\frac{p}{p_0} \right)^{(\gamma-1)/\gamma} \right]} = f(p_0, p, T_0) \quad (10)$$

Finally, the mass flow can be obtained by introducing the equation of state of a perfect gas and equation (10) in the continuity equation for a one-dimensional steady flow

$$\dot{m} = \rho VA = \frac{p}{RT} VA = f(p_0, p, T_0) \quad (11)$$

With regard to the *power input* provided by the fluid, it can be defined [35] as

$$P_{\text{input}} = Q \cdot p_{01} \quad (12)$$

Q being the volume flowrate calculated with the parameters measured at the inlet duct and p_{01} the total pressure obtained there.

5.2 Pressure losses before the nozzle

p_{01} was measured by a Pitot tube placed in a fitting right before the entrance to the nozzle inlet. There were some losses in the total pressure before reaching this point due to a series of contractions and enlargements in the fittings after the gas cylinder. These did not affect the reliability of the measured p_{01} , since it was measured downstream of them; however, as the total pressure after the gas cylinder was known and the dimensions of the changes in the diameter of the inlet duct were also known, a simple calculation for the drop in total pressure was carried out by using the equation

$$\Delta p_{0, \text{loss}} = \sum K_i \frac{1}{2} \rho V^2 \quad (13)$$

The values of K were obtained from reference [35].

The calculated pressure drop was within 5 per cent of the measured difference in total pressure between the gas cylinder and the nozzle inlet. This provides confidence in the measured value of p_{01} .

5.3 Nozzle

At the inlet of the nozzle, an estimated value of the stagnation pressure p_{01} and the stagnation temperature T_{01} are known. The static pressure at the outlet of the nozzle, p_2 , is estimated by means of the static pressure measurements in a number of circumferential positions inside the housing. As explained in section 3, two sets of pressure tapings were placed in the periphery of the housing, forming two parallel planes that were covered by the jet of the nozzle. Each set had three tapings, two of them being placed after and before the jet, and as close to it as possible, and the third tapping placed opposite to the outlet of the nozzle (Fig. 2(b)). The estimated static pressure at the outlet of the nozzle was then calculated by obtaining the tendency with the angle of measurement and extrapolating for that point.

An expression to deduce the total pressure in a compressible flow is outlined in references [30] and [36]. The expression is

$$p_{02} = p_2 \left[\frac{1}{2} + \sqrt{\frac{1}{4} + \left(\frac{\gamma - 1}{2\gamma} \right) \left(\frac{\dot{m}}{A_2 p_2} \right)^2 (RT_{02})} \right]^{\gamma/(\gamma-1)} \\ = f(p, \dot{m}, A, T_{02}) \quad (14)$$

This equation can be used to estimate the total pressure after the nozzle, since at that point all four parameters that determine p_{02} are known.

In order to have an approximate idea of the efficiency of the nozzle, by knowing the estimated total pressures for both inlet and outlet, the losses in the expansion can be analysed. As explained by Mattingly [9], the main losses in a nozzle are usually related to the loss in the total pressure from inlet to outlet, as well as to the over or under expansion

$$\pi_N = \frac{p_{02}}{p_{01}} < 1 \quad (15)$$

Another useful parameter to estimate losses in the nozzle is the loss coefficient, which, as outlined by Cohen in reference [10], expresses the proportion of energy degraded by friction

$$Y_N = \frac{(p_{01}/p_{02}) - 1}{1 - (p_2/p_{02})} \quad (16)$$

A typical value of the loss coefficient for gas turbine nozzles is $Y_N = 0.05$ [10].

As Shapiro explains in reference [37], the boundary layer is a critical factor for very small nozzles, since in this case its thickness can be as large as the channel, and this may decrease the efficiency. Therefore, this is one more thing to take into account when studying the performance of the nozzle for the Tesla turbine. Higher velocities of the flow will lead to higher

Reynolds numbers and thus to smaller thicknesses of the boundary layer, making it possible to reach higher efficiencies in the nozzle.

5.4 The turbine as a whole: power and efficiency

The conditions at the inlet of the rotor are assumed to be the same as those at the outlet of the nozzle; hence as explained before, properties at this point such as T_{02} ($T_{02} = T_{01}$), p_2 , and p_{02} can be determined. In addition, at the outlet of the rotor (point 3) T_{03} , p_3 , and p_{03} are measured. The mass flow can be recalculated at the outlet, applying the continuity equation, in order to see whether there has been any important leakage in the system.

The ideal power that should be developed by the turbine (isentropic power) is

$$\dot{W}_{\text{isen}} = \dot{m}c_p(T_{01} - T'_{03}) \quad (17)$$

where the ideal outlet temperature can be calculated by analysing the isentropic expansion in the rotor

$$T'_{03} = T_{02} \left(\frac{p_{02}}{p_{03}} \right)^{(1-\gamma)/\gamma} = T_{02} \left(\frac{p_{02}}{p_{03}} \right)^{(1-\gamma)/\gamma} \quad (18)$$

The output power due to the actual enthalpy drop is

$$\dot{W}_{\text{en}} = \dot{m}c_p(T_{01} - T_{03}) \quad (19)$$

And then, the efficiency of the turbine defined as the ratio of the output power due to the enthalpy drop and the power involved in the corresponding isentropic process is

$$\eta_{\text{en,isen}} = \frac{\dot{W}_{\text{en}}}{\dot{W}_{\text{isen}}} = \frac{T_{01} - T_{03}}{T_{01} - T'_{03}} \quad (20)$$

Moreover, the efficiency can also be defined as the ratio of the actual power obtained by means of the angular acceleration method and the power involved in the corresponding isentropic process

$$\eta_{\Omega,\text{isen}} = \frac{\tau\omega}{\dot{m}c_p(T_{01} - T'_{03})} \quad (21)$$

A third way to define the efficiency of the Tesla disc turbine is as the ratio of the actual power obtained by means of the angular acceleration method and the power of the input stream (equation (12))

$$\eta_{\Omega,\text{stream}} = \frac{\tau\omega}{Qp_{01}} \quad (22)$$

Previous researchers have used various ways to define the efficiency of a Tesla disc turbine as outlined in Table 1.

It has been explained in section 4.2 that there are uncertainties in the measurement of pressure and

Table 1 The definition of efficiency as used by previous researchers

Armstrong [5]	Rice [6]	Davydov and Sherstyuk [21]	Roddy <i>et al.</i> (for a pump) [35]
$\eta = \frac{P_{\text{Output}}}{h_1 - h'_3}$	$\eta = \frac{P_{\text{mechanical energy}}}{P_{\text{Isentropic expansion of the compressed air}}}$	$\eta = \frac{T_0 - T_3}{T_0(1 - p_3/p_0)}$	$\eta = \frac{P_{\text{delivered to the fluid}}}{P_{\text{shaft input}}} = \frac{\rho g H Q}{\tau \omega}$

temperature at the outlet of the current Tesla turbine due to the complexity of the exhaust flow. For this reason, the values of $\eta_{\Omega, \text{stream}}$ defined by equation (22) are used to represent the efficiency in the results given in this article; this definition is analogous to that employed by Roddy *et al.* [35].

6 RESULTS

Figure 5 shows the measured results of the current disc turbine with four discs of 92 mm diameter. The angular acceleration method described in section 3.3 was used to determine the accelerating and frictional torques, and the rotational speed is measured by an optical sensor (section 3.2). Figure 5(a) shows the variation of the actual torque (and its components) with rotational speed. Figure 5(b) shows the variation of the actual output power and the efficiency.

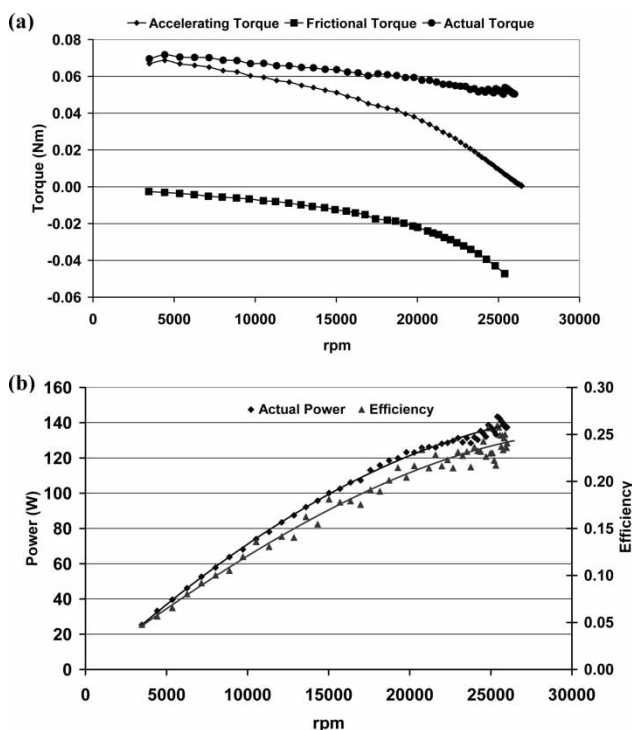


Fig. 5 Variation of output torque, power, and efficiency of the turbine as a function of angular speed (using four discs, obtained at an input total pressure of 3.9 bar). (a) Torques obtained by applying the angular acceleration method. (b) Actual power and efficiency

6.1 Output torque, power, and efficiency

The output torque decreases with increasing angular speed. The output power and efficiency initially increase with increasing angular speed before they reach a maxima. The maximum power reached by the present turbine was 140 W (0.2 hp), at 25 000 r/min, at which the turbine reached a steady state on its own, without using the eddy-current brake to load it. The efficiency of the turbine at this operating point is approximately 25 per cent. These conditions were obtained when a total pressure of 3.8 bar was applied at the inlet of the nozzle.

A Tesla turbine has many variables, e.g. disc diameter, disc thickness, number of discs used, disc spacing, nozzle design (e.g. number and circumferential positions of the nozzles, design of a plenum chamber, etc.), and design of the outlet. The various previous studies are all different in these respects from one another or from the design used for the present study. Indeed, we did not find any publication in which any results have been compared with those from another study. Although a direct comparison is not possible, the trends of the various curves in Fig. 5 are similar to the results given in the previous studies [5, 7]. The physical reasoning behind these trends can be explained in the following manner.

In the disc turbine, any relative velocity of the fluid across the discs causes a viscous drag force that accelerates the rotor. As the angular speed of the rotor increases, the viscous drag force decreases. Therefore, for a fixed inlet pressure (that controls the fluid jet speed at the inlet to the rotor), the torque decreases with increasing angular speed of the rotor, as seen in Fig. 5. Theoretical calculations by Beans [7] for laminar and turbulent flows through the disc spaces showed that the theoretically predicted torque decreases linearly with increasing angular speed (the magnitudes of the theoretical and experimental values of the torque in Beans' study were significantly different, but the same linear trend was observed in both curves).

Since output power is equal to output torque multiplied by angular speed, initially the output power of a disc turbine increases (non-linearly) with increasing angular speed as seen in Fig. 5. After reaching the maximum value, the output power of a disc turbine would decrease with any further increase in angular speed (as shown in reference [7]). Here a simple explanation for this behaviour of the output power of a disc turbine is provided. In the last paragraph, it is shown, from theoretical considerations, that $\tau \approx \tau_0 - c\omega$, where τ_0

and c are constants. Therefore, $P = \tau\omega \approx \tau_0\omega - c\omega^2$. Hence, a maxima in the power curve is achieved. In the present study, when the output power was close to its maximum value, the angular speed became high for the friction in the bearings, etc. to be of such value that the rotor achieved a steady state (i.e. the angular speed could not increase beyond the point of maximum power).

The diameter of the discs used in the present study is 92 mm; this is much smaller than the dimensions used in most of the previous studies. For example, Tesla himself used a disc diameter of 152.4 mm [3], Armstrong [5] used 177.8 mm, Beans [7] used 152.4 mm, and Rice [6] used 177.8 and 203.8 mm. The current machine (with a small disc diameter) therefore presented greater challenges in terms of measurement techniques since the torque is even smaller and the maximum angular speed is higher than that encountered in previous studies. The method of acceleration, developed by us for small disc turbines and described in section 3.3, needs to be mentioned in this respect. The attraction of the method lies in its simplicity and accuracy: an (inexpensive) optical sensor is used to obtain all three important parameters: angular speed, output torque, and output power.

The efficiency values shown in Fig. 5(b) are calculated by equation (22). The values of power shown in Fig. 5(b) are obtained from $P = \tau_{\text{actual}}\omega = (\tau_{\text{accelerating}} + |\tau_{\text{frictional}}|)\omega$. The accelerating torque $\tau_{\text{accelerating}}$ and the frictional torque $\tau_{\text{frictional}}$ are shown as functions of angular speed in Fig. 5(a). It is seen that the frictional torque (due to friction in the shaft bearings, etc.) in the present assembly is high and it increases rapidly with angular speed. At the maximum value of the angular speed shown in Fig. 5, the rotor assembly reached a steady state so that all power produced by the Tesla turbine was consumed at the shaft bearings. While evaluating the fluid dynamic performance of the Tesla turbine itself, it did not seem fair to charge the mechanical inefficiency of the bearings on the turbines, and hence in Fig. 5(b) we have shown the power that would have been available as output if the bearings were perfect (the bearing performance can be improved independently of the Tesla turbine, for example, using a higher grade bearing, better lubrication, a magnetic bearing, etc.). The corresponding efficiency shown in Fig. 5(b) can thus be considered to be a sort of internal fluid dynamic efficiency of the Tesla turbine. (In this respect, the efficiency shown here is similar to 'indicated efficiency' in the context of a reciprocating machine. Of course, it is easy to calculate the variation of $\tau_{\text{accelerating}}\omega$ if one is interested in the net shaft power available after the bearings.)

In section 4.2, the uncertainties in the measurement of pressure and temperature at the outlet due to the complexity of the exhaust flow are described. These inaccuracies would have affected seriously the isentropic efficiency, and that is why those results are

not shown in this article. The performance results shown in Fig. 5 are not affected by uncertainties in outlet measurements, since both the output torque and power are obtained from the angular acceleration method (section 3.3) and the efficiency is calculated from equation (22). According to equation (2), the accuracy of the measured torque depends on the accuracy of the moment of inertia I and the accuracy of measured angular speed ω . I is calculated by the Autodesk Inventor program from the original CAD files used for manufacturing the rotating parts, and hence is determined reliably. The maximum error in determining the revolutions per minute from the signal given by the optical sensor is specified in the manual of the data logger as ± 0.01 per cent. An error analysis involving equations (2) and (1) suggests that $d\tau/\tau \approx d\omega/\omega$ and $dP/P \approx 2 d\omega/\omega$. Hence, the torque and output power shown in Fig. 5 are quite accurate. The efficiency shown in Fig. 5 is calculated from equation (22). The accuracy of the numerator in equation (22) has already been described. The accuracy of the denominator depends on the accuracy of inlet total pressure p_{01} and volume flowrate Q . The manual of the Scanivalve specifies the error of the pressure measurement as ± 0.1 per cent FS, i.e. ± 0.05 psi (± 0.00345 bar). The main uncertainty is in the determination of Q since it was not measured directly but was estimated as the product of velocity and cross-sectional area of the inlet pipe. The average velocity is estimated by the one-dimensional gas dynamic approximation, equation (10), which depends on measured values of total pressure, static pressure, and total temperature (according to the manual of the data logger and the specification IEC 584-2 for a type-K thermocouple, the maximum error is $\pm(1 + 1.5)^\circ\text{C}$, i.e. $\pm 2.5^\circ\text{C}$). We have already mentioned that it is desirable to have an independent measurement of volume or mass flowrate and we are currently exploring suitable methods for the future continuation of the project.

6.2 Variation of efficiency with different parameters

Using the flexibility for changing parameters that the turbine used in this investigation permits, the efficiency was obtained by varying nozzle width, nozzle angle, disc spacing, and number of discs. It was found that the width of the nozzle did not influence the efficiency significantly. The optimum angle of injection of the fluid was found to be nearly tangential, although between 5° and 15° the efficiency was almost constant. As far as the disc spacing is concerned, the maximum efficiency was reached for a disc spacing of 0.6 mm, decreasing rapidly for spacings < 0.4 mm and > 1 mm. Finally, the efficiency increased when the number of discs was increased.

6.3 Losses in the nozzle

The values of two loss parameters (equations (15) and (16)) for the nozzle were determined in order to assess the influence of this loss on the overall efficiency of the disc turbine. The value of the total pressure at the outlet of the nozzle, p_{02} , is estimated by means of equation (14), as explained before in section 5.2. The results obtained for the loss parameters are given in Table 2.

These results show that there is a large loss of total pressure, giving rise to a high value of the loss coefficient Y_N (compare this with a typical value of the loss coefficient for gas turbine nozzles, which is usually about $Y_N = 0.05$ [10]). We are exploring the nozzle design and our current team members are planning to conduct specific tests to study nozzle performance and possible ways of improving it. However, our findings are in line with a general comment made by Rice [4] about the low efficiencies of the nozzles in Tesla turbines, even though Rice does not quote any numerical value for the loss coefficient. In reference [4] Rice writes:

In general, it has been found that the efficiency of rotor can be very high, at least equal to that achieved by conventional rotors. But it has proved very difficult to achieve efficient nozzles in the case of turbines. [...] As a result, only modest machine efficiencies have been demonstrated.

The results given in Table 2 show that the losses in the nozzle decrease when the velocity increases; a contributory factor for this effect has been explained before in section 5.

In order to double-check the validity of these results, a different test was carried out; the rotor and the base plate were taken out, so that the housing was open and it was possible to access the outlet of the nozzle directly, as can be seen in Fig. 1(c). Then, the inlet pipe was connected directly to the inlet of the nozzle and a Pitot tube was placed at the outlet. This made it possible to measure the total pressure at the outlet of the nozzle directly; this experimental result for p_{02} matched well with the estimated value from equation (14) (with which Table 2 has been constructed). It can therefore be confirmed that the high loss in the nozzle contributes strongly to the rather low efficiency of the turbine.

Even though the efficiency of a Tesla turbine is generally low, it may still find use in special areas because of its several attractive features. The first advantage is the simplicity of its design and manufacture. It is

also inexpensive. The turbine can be useful for situations involving small shaft power, very viscous fluids or non-Newtonian fluids, or non-conventional fuels (e.g. reference [38] gives a feasibility report on the use of Tesla turbines with biomass as the fuel). It is believed that Tesla turbines can cope better with particle-laden two-phase flows [4]. (References [39] to [43] describe the general aspects of two-phase flows).

6.4 Pressure distribution inside the housing

In order to check the efficacy of the sealing between the rotor and the end wall of the housing and whether this was causing part of the fluid injected by the nozzle to bypass the rotor, a set of three tappings was placed circumferentially in a plane parallel to the end wall of the housing, and close to it. The pressures measured there were compared with the readings obtained from the other two sets of tappings, outlined in section 3, which are situated within the axial bounds of the rotor. The results show that the pressures at the end wall of the housing were higher than the atmospheric pressure, and in the same range as those obtained in the tappings under the influence of the jet from the nozzle. Beans [7] suggested that part of the jet, in his turbine, went into the gap between the rotor and the housing. While we tried to minimize this unwanted flow of the jet into the gap, more detailed experiments are necessary to establish whether there may be a recirculating flow within the gap.

7 CONCLUSIONS

The design and manufacture of a Tesla disc turbine and of a flexible test rig to study systematically the performance of the turbine are described. Experimental results for a 92 mm diameter turbine are presented, which shows the variation of torque, output power, and efficiency as a function of angular speed. Measurements of total pressure, temperature, and static pressure are also taken at many locations at the inlet, outlet, and inside the housing for an understanding of the thermo-fluid dynamics of the machine. Many design considerations and operational experiences are discussed.

Several procedures for measuring torque and power are considered and implemented for cross-checking the measured values. Difficulties with many methods, which arise as a result of the high revolutions per minute and low torque output of the Tesla disc turbine, still remain. We have developed a new method, the angular acceleration method, for measuring the torque and power in a Tesla turbine (section 3.3). This proved to be a successful method; it is also the easiest and the most inexpensive of the available methods since the angular speed, output torque, and output power are all measured by an optical sensor.

Table 2 Loss parameters for the nozzle

Inlet total pressure	π_N	Y_N	V_2 (m/s)
3.0 bar	0.803	0.488	322.65
3.5 bar	0.820	0.407	346.07

Present experiments showed that the losses occurring in the nozzle are large and hence this needs to be tackled for improving the overall efficiency of the Tesla disc turbine. The output flow was found to be complex and more experiments (and probably an improved design) are necessary to assess whether a meaningful quasi-one-dimensional approach is feasible for this flow and to resolve the difficulties of measurement of total pressure and temperature at the outlet.

ACKNOWLEDGEMENTS

The authors are grateful to, among others, Keven Chappell, Sam Beale (Rolls-Royce), Lindsay Clare, Steve Macqueen, Sandy Mitchell, Steve Burrow, Sam McGarey, Peter Monson, and the technicians of the engineering faculty of the University of Bristol.

REFERENCES

- 1 **Tesla, N.** *Turbine*. US Pat. 1 061 206, May 1913.
- 2 **Tesla, N.** *Fluid propulsion*. US Pat. 1 061 142, May 1913.
- 3 **Cairns, W. M. J.** *The tesla disc turbine*, 2003 (Camden Miniature Steam Services, Great Britain).
- 4 **Rice, W.** Tesla turbomachinery. In *Handbook of turbo-machinery* (Ed. E. Logan), 2003 (Marcel Dekker, New York).
- 5 **Armstrong, J. H.** *An investigation of the performance of a modified Tesla turbine*. PhD Thesis, Faculty of the Division of Graduate Studies, Georgia Institute of Technology, June 1952.
- 6 **Rice, W.** An analytical and experimental investigation of multiple-disk turbines. *J. Eng. Power*, 1965, **87**(1), 29–36.
- 7 **Beans, E. W.** Investigation into the performance characteristics of a friction turbine. *J. Spacecr.*, 1966, **3**(1), 131–134.
- 8 **Hasinger, S. H.** and **Kehrt, L. G.** Investigation of a shear-force pump. *J. Eng. Power*, 1963, **85**(3), 201–207.
- 9 **Mattingly, J. D.** *Elements of gas turbine propulsion*, 1996 (McGraw Hill International Editions, Singapore).
- 10 **Cohen, H., Rogers, G. F. C., and Saravanamuttoo, H. I. H.** *Gas turbine theory*, 4th edition, 1996 (Longman Group Ltd, Cornwall).
- 11 **Guha, A.** Optimisation and design of aero gas turbine engines. *Aeronaut. J.*, 2001, **105**(1049), 345–358.
- 12 **Guha, A.** Performance and optimization of gas turbines with real gas effects. *Proc. IMechE, Part A: J. Power and Energy*, 2001, **215**(4), 507–512. DOI: 10.1243/0957650011538631.
- 13 **Guha, A.** An efficient generic method for calculating the properties of combustion products. *Proc. IMechE, Part A: J. Power and Energy*, 2001, **215**(3), 375–387. DOI: 10.1243/0957650011538596.
- 14 **Guha, A.** Optimum fan pressure ratio for bypass engines with separate or mixed exhaust streams. *AIAA J. Propuls. Power*, 2001, **17**(5), 1117–1122.
- 15 **Guha, A.** Effects of internal combustion and non-perfect gas properties on the optimum performance of gas turbines. *Proc. IMechE, Part C: J. Mechanical Engineering Science*, 2003, **217**(9), 1085–1099. DOI: 10.1243/095440603322407317.
- 16 **Entrican, J. R.** *Tesla turbine*. US Pat. Application Publication, December 2002.
- 17 **Peterson, G. L.** *A new advance in Tesla turbine theory*, 2007, available from the Twenty First Century books site, www.tfcbooks.com/articles/tdt6.htm.
- 18 **Peterson, G. L.** *Nikola Tesla's disk turbine*, 2007, available from the Twenty First Century books site, www.tfcbooks.com/articles/tdt7.htm.
- 19 **Allan, S. D.** *Tesla turbine: engine of the 21st Century?* 2007, available from the Pure Energy Systems site, http://pesn.com/Radio/Free_Energy_Now/shows/2007/04/14/9700225_KenReili_TeslaTurbine/.
- 20 **Swithenbank, A.** *The Tesla boundary layer turbine*, January 2008, available from the Stanford University site, www.stanford.edu/~hydrobay/lookat/tt.html#sect-1-a.
- 21 **Davydov, A. B.** and **Sherstyuk, A. N.** Experimental research on a disc microturbine. *Russ. Eng. J.*, 1980, **60**(8), 19–22.
- 22 Scanivalve Corp. *ZOC 22B electronic pressure scanning module. Instruction and Service Manual*, 2005, available from Scanivalve site www.scanivalve.com.
- 23 Agilent Technologies. *Agilent 34970A Data acquisition/switch unit. user's guide*, 2006, available from Agilent site www.agilent.com.
- 24 **Lee, K.** and **Park, K.** Optimal robust control of a contactless brake system using an eddy current. *Mechatronics*, 1999, **9**, 615–631.
- 25 **Faupel, J. H.** *Engineering design: a synthesis of stress analysis and materials engineering*, 1964 (John Wiley and Sons Inc., New York).
- 26 **Anwar, S.** A parametric model of an eddy current electric machine for automotive braking applications. *IEEE Trans. Control Syst. Technol.*, 2004, **12**(3), 422–427.
- 27 **Simeu, E.** and **Georges, D.** Modelling and control of an eddy current brake. *Control Eng. Pract.*, 1996, **4**(1), 19–26.
- 28 **McGarey, S.** and **Monson, P.** Performance and efficiency of disk turbines, Final Research Project report, University of Bristol, 2007.
- 29 **Pablo Hoya, G.** Performance and efficiency of disk turbines, Final Research Project report, University of Bristol, 2008.
- 30 **Benedict, R. P.** *Fundamentals of temperature, pressure, and flow measurements*, 1977 (John Wiley & sons, New York).
- 31 **Dreco, D.** *Eddy-current brake device*, US Pat. Application Publication, 2001.
- 32 **Gindy, S. S.** Force and torque measurement, a technology overview. Part II-torque. *Exp. Tech.*, 1985, **9**(7), 9–14.
- 33 **Fleming, W. J.** Automotive torque measurement: a summary of seven different methods. *IEEE Trans. Veh. Technol.*, 1982, **VT-31**(3), 117–124.
- 34 **Massey, B.** *Mechanics of fluids*, 8th edition, 2006 (Taylor & Francis, Oxon).
- 35 **Roddy, P. J., Darby, R., Morrison, G. L., and Jenkins, P. E.** Performance characteristics of a multiple-disk centrifugal pump. *J. Fluids Eng.*, 1987, **109**, 51–57.
- 36 **Benedict, R. P., Wyler, J. S., Dudek, J. A., and Gleed, A. R.** Generalized flow across an abrupt enlargement. *Trans. ASME, J. Eng. Power*, 1976, **98**, 327–334.

- 37 Shapiro, A. H. *The dynamics and thermodynamics of compressible fluid flow*, 1st edition, 1953, vol. I (The Ronald Press Company, New York).
- 38 Schmidt, D. D. Biomass Boundary Layer Turbine Power System, Energy Innovations Small Grant (EISG) Program, 2002.
- 39 Guha, A. A unified theory of aerodynamic and condensation shock waves in vapour-droplet flows with or without a carrier gas. *Phys. Fluids*, 1994, **6**(5), 1893–1913.
- 40 Guha, A. Structure of partly dispersed normal shock waves in vapour-droplet flows. *Phys. Fluids A*, 1992, **4**(7), 1566–1578.
- 41 Guha, A. Jump conditions across normal shock waves in pure vapour-droplet flows. *J. Fluid Mech.*, 1992, **241**, 349–369.
- 42 Guha, A. A unified theory for the interpretation of total pressure and temperature in two-phase flows at subsonic and supersonic speeds. *Proc. R. Soc.*, 1998, **454**, 671–695.
- 43 Guha, A. Computation, analysis and theory of two-phase flows. *Aeronaut. J.*, 1998, **102**(1012), 71–82.

APPENDIX

Notation

a	length of the pole of the electromagnet (perpendicular to radius of disc)
A	area
b	width of the pole of the electromagnet (parallel to radius of disc)
c_p	specific heat capacity at constant pressure
C	compensating factor for braking torque
d	thickness of the disc of the eddy-current brake
g	acceleration due to gravity
i	applied current
I	moment of inertia
K	head loss coefficient
l_g	distance of air gap
\dot{m}	mass flow
M	Mach number
N	number of turns
p	pressure
P	power
Q	volume flowrate

r	radius of the disc
R	gas constant
\mathfrak{R}	distance between the centre of the disc and the centre of the pole
S	surface area of the pole of the electromagnet
S_f	safety factor
T	temperature
v	voltage
V	absolute velocity
α	angular acceleration
β	compensating factor for braking torque
γ	ratio of specific heats
η	efficiency
μ_0	permeability of air
ν	Poisson's ratio
ρ	density
σ	electrical conductivity
σ_w	working stress = σ_y/S_f
σ_y	yield stress
τ	torque
τ_b	braking torque
τ_i	braking torque constant
ω	rotor angular velocity

Subscripts

0	stagnation conditions
1	conditions at the inlet of the nozzle
2	conditions outlet of the nozzle/inlet of the rotor
3	conditions at the exhaust from the turbine
en	power due to enthalpy drop
isen	power of the isentropic process
stream	power due to the input stream of fluid
Ω	output from the angular acceleration method
i	inner
o	outer

Superscript

'	ideal (isentropic) conditions
---	-------------------------------